OPEN ACCESS
IOP Publishing
Measurement Science and Technology
Meas. Sci. Technol. **33** (2022) 085020 (16pp)
https://doi.org/10.1088/1361-6501/ac6f45

GBDM+: an improved methodology for a GNSS-based distance meter

Sergio Baselga*, Luis García-Asenjo, Pascual Garrigues and Raquel Luján

Cartographic Engineering, Geodesy and Photogrammetry Department, Universitat Politècnica de València, Camino de Vera s/n, 46022 Valencia, Spain

E-mail: serbamo@cgf.upv.es

Received 3 February 2022, revised 27 April 2022
Accepted for publication 12 May 2022
Published 25 May 2022

Abstract

The determination of distances consistent with the definition of the base unit of length in the International System of Units (SI), the SI meter, with uncertainties of less than 1 ppm up to 5 km in the open air is a current challenge that is being increasingly required for different applications, including the determination of local ties, calibration baselines, and high precision geodetic metrology in singular scientific and engineering projects. The required knowledge of the index of refraction of the propagating medium at the same level of 1 ppm is a hard limit to the use of precise electronic distance meters (EDMs), which has motivated the recent development of new two-color, refractivity compensated, EDM prototypes. As an alternative, the use of global navigation satellite systems (GNSS) could benefit from their high scale stability although the lack of appropriate estimation of the uncertainties in their sources of error and their unknown propagation into the final result during the data processing has prevented a rigorous uncertainty analysis and, therefore, the use of GNSS for absolute distance determination. Stemming from our initial methodology for a GNSS-based distance meter (GBDM) that was restricted to relatively horizontal baselines and distances up to 1 km only, we have improved the method so that its application range is extended to baselines of up to 5 km with a possibly significant height difference so that it provides the final baseline distance with the corresponding uncertainty derived from the uncertainties in the different error sources rigorously propagated through the equations by which the distance is finally determined. This improved methodology, named as GBDM+, constitutes a significant step forward in the application of GNSS to open air length metrology.

Keywords: global navigation satellite systems (GNSS), length, metrology

(Some figures may appear in colour only in the online journal)

1. Introduction

Length metrology is concerned with the realization, maintenance and dissemination of the SI meter, which is defined as the length of the path travelled by light in vacuum during a time interval with duration of 1/299 792 458 of a second [1]. This realization is done with uncertainties of the order of 10^{-12} ($k = 1$) for short distances under laboratory conditions by means of laser interferometers with stabilised frequencies, but suffers a considerable loss of accuracy when transferred to outdoor facilities.

Absolute distance determination, or the determination of distances consistent with the SI meter definition, with an uncertainty of less than 1 part per million (1 ppm) is being increasingly required in the open air for different applications,

* Author to whom any correspondence should be addressed.

including the determination of local ties in Fundamental Geodetic Observatories [2], high precision geodetic metrology in singular scientific projects, such as the European Organization for Nuclear Research (CERN) site for the survey and alignment of the components of accelerators, experiments and transfer lines [3], especially in views of the construction of the Future Circular Collider, a 100 km-length ring aiming at reaching collision energies of 100 TeV in the search for new physics, where geodetic surveillance with the highest accuracy will be required, and calibration baselines, such as the Nummela standard baseline [4], which, in turn, are used to accurately transfer the SI meter to engineering projects where a scale control is crucial, e.g. deformation monitoring of civil infrastructures, landslides and rockfalls [5]. The use of high precision electronic distance meters (EDMs) for this purpose is limited by the required determination of the index of refraction along the light path with an uncertainty below 1 ppm, which is a hard task in the open air even for lengths of only several hundred meters, since it has to be deduced from the accurate measurement of atmospheric parameters representative to the entire light path. This is why new techniques and prototypes, such as two-color laser telemeters are being developed [6].

A possible alternative to these is the use of global navigation satellite systems (GNSS) to develop a GNSS-based distance meter (GBDM). GNSS scale is consistent with the SI meter by its maintenance by means of the use of atomic clocks and has been demonstrated to be worldwide stable at the level of 0.001 ppm (or 1 ppb) [7, 8]. The Joint Research Project (JRP) SIB60 Metrology for long distance surveying project [2], a joint effort of a consortium of European metrology institutes and universities, addressed this possibility and summarized their research in their *Good practice guide for high accuracy global navigation satellite system based distance metrology* [9]. Among the conclusions drawn, they pointed out that the 'propagation of the signal through the ionosphere and troposphere, effect of multipath, antenna phase center variations (PCVs) and other sources of error are not controllable and are mostly unknown during the data processing. Although one can estimate the magnitude of these variables in the analysis, uncertainties of these estimations are mostly unknown, and especially their propagation into the final results'. They also remarked that the user has little information on the propagation of uncertainties when using standard software packages. This prevents, they concluded, a stringent uncertainty analysis of a distance measurement performed by GNSS.

The JRP SIB60 Metrology for long distance surveying project was concerned with lengths up to 1 km. Recently, this consortium renewed and united in a new research project, GeoMetre [6, 10], that is aimed at improving the traceability of geodetic references to the SI meter definition with the focus extended to lengths up to 5 km, including the development of novel distance meters and a novel strategy for GNSS-based distance determination for this range. The presentation of this strategy is the objective of the current paper, a strategy which provides the user with the detailed analysis of the uncertainty in the different error sources and its propagation through the particular double-differenced equations up to the determination of the baseline distance, whose final value can be now accompanied with the corresponding uncertainty budget, something which is not possible to be carried out by the existing software packages and has prevented so far the use of GNSS techniques for metrological purposes.

We started our research in submillimetric GNSS-based length determination, first analyzing the inner consistency of results [11], then with a first comparison with respect to a value obtained by absolute-scale transfer from the Nummela baseline with a Mekometer ME5000 [12], a type of comparison that has also been done by other authors (e.g. [13]). We explored different strategies to mitigate noise, especially multipath [12, 14, 15] and finally came with a working scheme for a GBDM [16]. This method was, however, restricted to relatively horizontal baselines with distances up to 1 km only and, correspondingly, had several simplifications (such as no correction of double-differenced tropospheric and ionospheric delays). In accordance with the objectives of the Geometre project, we want to improve the method now so that its application range can be extended to baselines of up to 5 km with significant (or not) height difference. The improved methodology for this GBDM will be referred to as GBDM+ two observation campaigs are planned during 2022 where the GBDM+ methodology will be contrasted with refractivity compensated two-color EDM prototypes in two singular sites: the CERN geodetic network and the European primary reference baseline EURO5000 [10].

In particular we are aiming at defining a relatively simple strategy for use in length metrology that is based as far as possible on the use of renowned standards both for files and solutions (such as Receiver Independent Exchange—RINEX—for GNSS data files, SP3 files as provided by the International GNSS Service—IGS—for final ephemerides of satellites, Antenna Exchange Format—ANTEX—files as provided by IGS for satellite antenna phase center offsets (PCOs) and variations and ANTEX files for individual antenna calibrations at the receiver ends) as well as an initial preprocessing with the online service CSRS-PPP version 3 [17], which is increasingly being used by the geodetic community and has some distinctive features over other solutions that may suggest its acceptance as a type of standard for precise point positioning (PPP). To start with, PPP with ambiguity resolution is automatically enabled in this processing, which is the best strategy to obtain reliable results [18]. Secondly, after uploading an observation RINEX file—not limited to 24 h as in other services—to the CSRS-PPP website, the service sends an email to the user with exhaustive information on the processing and results: station coordinates referred to the mean observation epoch with high quality (uncertainties typically of the order of some mm for 24 h observation files), excellent tropospheric estimates (see [18, 19]) along with their corresponding uncertainties, receiver clocks, observation residuals in L_1 and L_2 carrier phase frequencies, some detailed plots, etc.

Although the user could undoubtedly obtain this initial information—approximate coordinates, tropospheric delays,

clocks—from other sources ranging from the use of scientific packages (e.g. Bernese) to commercial solutions or user-developed software, the use of CSRS-PPP is here suggested as a simple, easy-to-use means to obtain a set of initial information that is both internally consistent as well as consistent with standard up-to-date IGS products.

In the following section we present the GBDM+ methodology. It is highlighted that its purpose is not only obtaining a value for the baseline distance but also its corresponding uncertainty as propagated from the corresponding uncertainties of the corrections of the different error sources rigorously propagated through the equations by which the distance is finally determined. This sets this methodology apart from other attemps than did not take into account the uncertainties in the corrections of every single error and their propagation through the particular equations leading to the resulting distance. That was precisely the reason that led to conclude the JRP SIB60 Metrology for long distance surveying group in their *Good practice guide for high accuracy global navigation satellite system based distance metrology* [9] that a rigorous uncertainty budget for the distance could not be provided. The situation is remedied with our GBDM+ methodology, which estimates not only the baseline distance but the contribution of each error source to this distance and the corresponding total uncertainty, which enables using the methodology for metrological purposes.

2. Methods

We start with a description of the GBDM+ mathematical model, which has been specially tailored to the optimal determination of the distance as a result of enabling the study of the impact of all relevant sources of error on the particular distance and the possible mitigation of their influence on the distance. Other parameters of the baseline (azimuth and height difference, or coordinate differences) are left outside the focus, so that they might not be optimally determined—if desired—by the current methodology. This is clearly at variance with the standard geodetic processing, which, in general, focuses on coordinate determination.

After introducing the GBDM+ model we will present a general scheme for uncertainty propagation from an error source in zero differences to double-differenced equations, first, and then to the final distance determined. This scheme will be conveniently particularized next to the existing relevant error sources.

As it is recalled in [9], the propagation of uncertainty from the different error sources to the final distance cannot be studied with standard software packages; the present derivation and directions of use constitute therefore a significant step forward in the application of GNSS to length metrology.

2.1. GNSS-based distance meter

The carrier phase observation equation for a receiver i and a satellite k can be written, slightly adapted from [16], as

$$\lambda\varphi_i^k = \rho_i^k + \lambda N_i^k + cdt_i - cdt^k - I_i^k + T_i^k + \mathrm{MP}_i^k + \delta_i - \delta^k + \varepsilon_i^k \tag{1}$$

where λ is the carrier wavelength, φ_i^k is the carrier phase in unit cycles, ρ_i^k is the geometric distance between satellite and receiver at the reception point of the antenna, N_i^k is the integer ambiguity, c is the light speed in vacuum, dt_i and dt^k are the receiver and satellite clock offsets, respectively, I_i^k and T_i^k are the slant ionospheric and tropospheric delays, respectively, MP_i^k is the carrier phase multipath error, δ_i and δ^k are hardware biases and initial carrier phase offsets in the receiver and the satellite, respectively, and ε_i^k is the remaining observation error.

Note that, contrary to other expressions that incorporate this error in the lumped term ε_i^k, this formulation explicitly includes a multipath term MP_i^k to highlight the existence of this error. Antenna PCO and variations are assumed to have been corrected with a model but these corrections are not regarded as exact so that their uncertainty will be assessed and then propagated to the final distance. This is explained later in the dedicated subsection.

Equation (1) models the actual GNSS observation and is often known as zero-differenced equation. In order to compute the unknown parameters one normally finds positioning approaches based on the difference of equations for two satellites and the same receiver, known as single-differenced equations, or, even more commonly in surveying, approaches based on the difference of equations for two satellites and two receivers, known as double-differenced equations. As acknowledged in [2], 'for single difference measurements other sources of uncertainty that usually cancel in the analysis based on double differences now dominate the uncertainty'. This is the main reason why we propose the use of double-differenced equations in the current method: diminishing the final uncertainty. As explained later, the relevant error sources will be estimated in zero differences along with their uncertainties, but these uncertainties will be then propagated to the double differences scheme used to compute the distance. It is worth noting that many double differenced errors do not cancel but get diminished only; correspondingly, uncertainties in the double differenced corrections will not be neglected (as is often encountered) but rigorously computed using the double difference scheme and then propagated to the final distance through the equations in use for the solution of the system of equations. This is certainly the only way to provide the final distance with its corresponding rigorously computed uncertainty budget.

The scheme of double differences for a pair of receivers i and j and a pair of satellites k and l, can be formed for the carrier phases as follows

$$\varphi_{ij}^{kl} = \varphi_j^l - \varphi_j^k - \varphi_i^l + \varphi_i^k. \tag{2}$$

Following the same notation for the rest of the parameters we can write

$$\lambda\varphi_{ij}^{kl} = \rho_{ij}^{kl} + \lambda N_{ij}^{kl} - I_{ij}^{kl} + T_{ij}^{kl} + \mathrm{MP}_{ij}^{kl} + \varepsilon_{ij}^{kl} \tag{3}$$

where common errors (clock offsets, hardware biases and initial carrier phase offsets) have cancelled.

Let us use some approximate coordinates for the receivers (from the preliminary PPP computation) along with coordinates for the satellites (from precise ephemerides). It is possible to linearly expand equation (3) in terms of the unknown corrections to the approximate coordinates of receivers, dX_i, dY_i and dZ_i, dX_j, dY_j and dZ_j, and write

$$\begin{aligned}\lambda\varphi_{ij}^{kl}-\rho_{ij0}^{kl}=\lambda N_{ij}^{kl}&+\left(\frac{\partial\rho_{ij}^{kl}}{\partial X_i}\right)_0 dX_i+\left(\frac{\partial\rho_{ij}^{kl}}{\partial Y_i}\right)_0 dY_i\\&+\left(\frac{\partial\rho_{ij}^{kl}}{\partial Z_i}\right)_0 dZ_i+\left(\frac{\partial\rho_{ij}^{kl}}{\partial X_j}\right)_0 dX_j+\left(\frac{\partial\rho_{ij}^{kl}}{\partial Y_j}\right)_0 dY_j\\&+\left(\frac{\partial\rho_{ij}^{kl}}{\partial Z_j}\right)_0 dZ_j-I_{ij}^{kl}+T_{ij}^{kl}+\mathrm{MP}_{ij}^{kl}+\varepsilon_{ij}^{kl}.\end{aligned}\tag{4}$$

In practice, for baselines up to tens of kilometers, two considerations are made with a completely negligible effect on the results. First, the derivatives of the satellite-to-receiver distances with respect to coordinates of i can be considered equal to the derivatives of the satellite-to-receiver distances with respect to coordinates of j so that it can be written

$$\begin{aligned}\lambda\varphi_{ij}^{kl}-\rho_{ij0}^{kl}=\lambda N_{ij}^{kl}&+\left(\frac{\partial\rho_{ij}^{kl}}{\partial X_j}\right)_0 (dX_i+dX_j)\\&+\left(\frac{\partial\rho_{ij}^{kl}}{\partial Y_j}\right)_0 (dY_i+dY_j)+\left(\frac{\partial\rho_{ij}^{kl}}{\partial Z_j}\right)_0 (dZ_i+dZ_j)\\&-I_{ij}^{kl}+T_{ij}^{kl}+MP_{ij}^{kl}+\varepsilon_{ij}^{kl}\end{aligned}\tag{5}$$

or

$$\begin{aligned}\lambda\varphi_{ij}^{kl}-\rho_{ij0}^{kl}=\lambda N_{ij}^{kl}&+\left(\frac{\partial\rho_{ij}^{kl}}{\partial X_j}\right)_0 dX_{ij}+\left(\frac{\partial\rho_{ij}^{kl}}{\partial Y_j}\right)_0 dY_{ij}\\&+\left(\frac{\partial\rho_{ij}^{kl}}{\partial Z_j}\right)_0 dZ_{ij}-I_{ij}^{kl}+T_{ij}^{kl}+MP_{ij}^{kl}+\varepsilon_{ij}^{kl}\end{aligned}\tag{6}$$

denoting by dX_{ij}, dY_{ij}, dZ_{ij} the combined effect of changes in coordinates of i and j, that is

$$dX_{ij}=dX_i+dX_j\tag{7}$$

$$dY_{ij}=dY_i+dY_j\tag{8}$$

$$dZ_{ij}=dZ_i+dZ_j.\tag{9}$$

A second consideration with a completely negligible impact on the results for baselines up to tens of kilometers is holding fixed the coordinates of one of the baseline endpoints, say i, so that $dX_i=dY_i=dZ_i=0$ in equations (7)–(9), and the displacement of coordinates (or the differential change in the baseline distance, for what matters in our case) is attributed to changes in coordinates of one station only, dX_j, dY_j, dZ_j.

Therefore, the double-differenced carrier phase equation model, as it is normally given in textbooks, reads

$$\begin{aligned}\lambda\varphi_{ij}^{kl}-\rho_{ij0}^{kl}=\lambda N_{ij}^{kl}&+\left(\frac{\partial\rho_{ij}^{kl}}{\partial X_j}\right)_0 dX_j+\left(\frac{\partial\rho_{ij}^{kl}}{\partial Y_j}\right)_0 dY_j\\&+\left(\frac{\partial\rho_{ij}^{kl}}{\partial Z_j}\right)_0 dZ_j-I_{ij}^{kl}+T_{ij}^{kl}+\mathrm{MP}_{ij}^{kl}+\varepsilon_{ij}^{kl}.\end{aligned}\tag{10}$$

We can group in the left-hand side of the equation all the parameters that could be determined somehow (we postpone to later sections of the paper the detailed explanation on the ways to do so), including in this category the integer ambiguity values, ionospheric and tropospheric delays and multipath errors and write the double differences equation as

$$\begin{aligned}&\lambda\varphi_{ij}^{kl}-\rho_{ij0}^{kl}-\lambda N_{ij}^{kl}+I_{ij}^{kl}-T_{ij}^{kl}-MP_{ij}^{kl}-\varepsilon_{ij}^{kl}\\&\quad=\left(\frac{\partial\rho_{ij}^{kl}}{\partial X_j}\right)_0 dX_j+\left(\frac{\partial\rho_{ij}^{kl}}{\partial Y_j}\right)_0 dY_j+\left(\frac{\partial\rho_{ij}^{kl}}{\partial Z_j}\right)_0 dZ_j.\end{aligned}\tag{11}$$

With equations of the type of equation (11) one gets a system of equations of the form

$$\boldsymbol{k}+\boldsymbol{r}=\boldsymbol{A}\boldsymbol{x}\tag{12}$$

where

$$\boldsymbol{k}=\begin{pmatrix}\lambda\varphi_{ij}^{kl(1)}-\rho_{ij0}^{kl(1)}-\lambda N_{ij}^{kl(1)}+I_{ij}^{kl(1)}-T_{ij}^{kl(1)}-\mathrm{MP}_{ij}^{kl(1)}\\ \lambda\varphi_{ij}^{km(1)}-\rho_{ij0}^{km(1)}-\lambda N_{ij}^{km(1)}+I_{ij}^{km(1)}-T_{ij}^{km(1)}-\mathrm{MP}_{ij}^{km(1)}\\ \vdots\\ \lambda\varphi_{ij}^{st(1)}-\rho_{ij0}^{st(1)}-\lambda N_{ij}^{st(1)}+I_{ij}^{st(1)}-T_{ij}^{st(1)}-\mathrm{MP}_{ij}^{st(1)}\\ \vdots\\ \lambda\varphi_{ij}^{kl(N)}-\rho_{ij0}^{kl(N)}-\lambda N_{ij}^{kl(N)}+I_{ij}^{kl(N)}-T_{ij}^{kl(N)}-\mathrm{MP}_{ij}^{kl(N)}\\ \vdots\\ \lambda\varphi_{ij}^{rt(N)}-\rho_{ij0}^{rt(N)}-\lambda N_{ij}^{rt(N)}+I_{ij}^{rt(N)}-T_{ij}^{rt(N)}-\mathrm{MP}_{ij}^{rt(N)}\end{pmatrix}\tag{13}$$

$$\boldsymbol{r}=\begin{pmatrix}-\varepsilon_{ij}^{kl(1)}\\ -\varepsilon_{ij}^{km(1)}\\ \vdots\\ -\varepsilon_{ij}^{st(1)}\\ \vdots\\ -\varepsilon_{ij}^{kl(N)}\\ \vdots\\ -\varepsilon_{ij}^{rt(N)}\end{pmatrix}\tag{14}$$

$$\boldsymbol{A} = \begin{pmatrix} \left(\frac{\partial \rho_{ij}^{kl}}{\partial X_j}\right)_0^{(1)} & \left(\frac{\partial \rho_{ij}^{kl}}{\partial Y_j}\right)_0^{(1)} & \left(\frac{\partial \rho_{ij}^{kl}}{\partial Z_j}\right)_0^{(1)} \\ \left(\frac{\partial \rho_{ij}^{km}}{\partial X_j}\right)_0^{(1)} & \left(\frac{\partial \rho_{ij}^{km}}{\partial Y_j}\right)_0^{(1)} & \left(\frac{\partial \rho_{ij}^{km}}{\partial Z_j}\right)_0^{(1)} \\ \vdots & & \\ \left(\frac{\partial \rho_{ij}^{st}}{\partial X_j}\right)_0^{(1)} & \left(\frac{\partial \rho_{ij}^{st}}{\partial Y_j}\right)_0^{(1)} & \left(\frac{\partial \rho_{ij}^{st}}{\partial Z_j}\right)_0^{(1)} \\ \vdots & & \\ \left(\frac{\partial \rho_{ij}^{kl}}{\partial X_j}\right)_0^{(N)} & \left(\frac{\partial \rho_{ij}^{kl}}{\partial Y_j}\right)_0^{(N)} & \left(\frac{\partial \rho_{ij}^{kl}}{\partial Z_j}\right)_0^{(N)} \\ \vdots & & \\ \left(\frac{\partial \rho_{ij}^{rt}}{\partial X_j}\right)_0^{(N)} & \left(\frac{\partial \rho_{ij}^{rt}}{\partial Y_j}\right)_0^{(N)} & \left(\frac{\partial \rho_{ij}^{rt}}{\partial Z_j}\right)_0^{(N)} \end{pmatrix} \tag{15}$$

$$\boldsymbol{x} = \begin{pmatrix} dX_j \\ dY_j \\ dZ_j \end{pmatrix} \tag{16}$$

for satellites *k, l, m, .., r, s, t*, and observation epochs (1), to (*N*). Note that, obviously, the same satellite pair may not be available in different epochs.

The system of equations in equation (12) is normally solved by least squares to yield a solution in the coordinate domain (dX_j, dY_j, dZ_j and then X_j, Y_j, Z_j, enabling one to obtain the baseline components $\Delta X = X_j - X_i$, $\Delta Y = Y_j - Y_i$ and $\Delta Z = Z_j - Z_i$). This is standard in the literature. We want to focus on the distance and its corresponding uncertainty, however, so we will deviate from the beaten track and propose a particular change of variable for directly evaluating the distance and its corresponding uncertainty.

Taking into account, first, that the relationship between the distance D, azimuth α and (local) height difference z, and the increments of coordinates *x, y, z* (or easting, northing, upping) in the local geodetic system can be written for differential values as

$$\begin{pmatrix} dD_{ij} \\ d\alpha_{ij} \\ dz_{ij} \end{pmatrix} = \boldsymbol{J} \begin{pmatrix} dx_{ij} \\ dy_{ij} \\ dz_{ij} \end{pmatrix} \tag{17}$$

with

$$\boldsymbol{J} = \begin{pmatrix} \frac{\partial D_{ij}}{\partial x_{ij}} & \frac{\partial D_{ij}}{\partial y_{ij}} & \frac{\partial D_{ij}}{\partial x_{ij}} \\ \frac{\partial_{ij}}{\partial x_{ij}} & \frac{\partial_{ij}}{\partial y_{ij}} & \frac{\partial_{ij}}{\partial z_{ij}} \\ \frac{\partial z_{ij}}{\partial x_{ij}} & \frac{\partial z_{ij}}{\partial y_{ij}} & \frac{\partial z_{ij}}{\partial z_{ij}} \end{pmatrix} = \begin{pmatrix} \frac{x_j - x_i}{D_{ij}} & \frac{y_j - y_i}{D_{ij}} & \frac{z_j - z_i}{D_{ij}} \\ \frac{y_j - y_i}{(x_j - x_i)^2 + (y_j - y_i)^2} & \frac{-(x_j - x_i)}{(x_j - x_i)^2 + (y_j - y_i)^2} & 0 \\ 0 & 0 & 1 \end{pmatrix} \tag{18}$$

and considering, second, that a rotation matrix relates the increments of coordinates *x, y, z* in the local geodetic system and the increments of Earth-Centered Earth-Fixed coordinates *X, Y, Z* in a global reference system (here the International Terrestrial Reference Frame, or equivalently, the IGbyy as given in the precise ephemerides file) [20] by

$$\begin{pmatrix} dx_{ij} \\ dy_{ij} \\ dz_{ij} \end{pmatrix} = \boldsymbol{R}^{\mathrm{T}} \begin{pmatrix} dX_{ij} \\ dY_{ij} \\ dZ_{ij} \end{pmatrix} \tag{19}$$

$$\boldsymbol{R}^{\mathrm{T}} = \begin{pmatrix} -\sin\lambda_j & \cos\lambda_j & 0 \\ -\sin\varphi_j\cos\lambda_j & -\sin\varphi_j\sin\lambda_j & \cos\varphi_j \\ \cos\varphi_j\cos\lambda_j & \cos\varphi_j\sin\lambda_j & \sin\varphi_j \end{pmatrix} \tag{20}$$

where we have taken *j* as the origin of the local system, something that should be done also for equation (18), which means computing the coordinates therein for the local geodetic system of *j*. Both equations (17) and (19) are invertible so that the relationships can also be written (note that the inverse of a rotation matrix is its transpose) as

$$\begin{pmatrix} dx_{ij} \\ dy_{ij} \\ dz_{ij} \end{pmatrix} = \boldsymbol{J}^{-1} \begin{pmatrix} dD_{ij} \\ d\alpha_{ij} \\ dz_{ij} \end{pmatrix} \tag{21}$$

$$\begin{pmatrix} dX_{ij} \\ dY_{ij} \\ dZ_{ij} \end{pmatrix} = \boldsymbol{R} \begin{pmatrix} dx_{ij} \\ dy_{ij} \\ dz_{ij} \end{pmatrix}. \tag{22}$$

By combining these two equations we can write

$$\begin{pmatrix} dX_{ij} \\ dY_{ij} \\ dZ_{ij} \end{pmatrix} = \boldsymbol{R}\boldsymbol{J}^{-1} \begin{pmatrix} dD_{ij} \\ d\alpha_{ij} \\ dz_{ij} \end{pmatrix}. \tag{23}$$

Recall that we assumed $dX_i = dY_i = dZ_i = 0$ in equations (7)–(9), so that we can write

$$\begin{pmatrix} dX_j \\ dY_j \\ dZ_j \end{pmatrix} = \boldsymbol{R}\boldsymbol{J}^{-1} \begin{pmatrix} dD_{ij} \\ d\alpha_{ij} \\ dz_{ij} \end{pmatrix}. \tag{24}$$

The changes in the distance from *i* to *j* (as well as the changes in the azimuth and height from *i* to *j*) can therefore be related to the changes in coordinates of *j*, dX_j, dY_j, dZ_j (assuming *i* is fixed) via equation (24).

We recall from equation (16) that he left-hand side of equation (24) is the unknown $\boldsymbol{x}$ of the system of equations in equation (12), which can be written now as

$$\boldsymbol{k} + \boldsymbol{r} = \boldsymbol{A}\boldsymbol{R}\boldsymbol{J}^{-1} \begin{pmatrix} dD_{ij} \\ d\alpha_{ij} \\ dz_{ij} \end{pmatrix}. \tag{25}$$

We can define a new matrix $\boldsymbol{B}$ and a new unknown vector $\boldsymbol{x}'$ as

$$\boldsymbol{B} = \boldsymbol{A}\boldsymbol{R}\boldsymbol{J}^{-1} \tag{26}$$

$$\boldsymbol{x}' = \begin{pmatrix} dD_{ij} \\ d\alpha_{ij} \\ dz_{ij} \end{pmatrix} \tag{27}$$

so that the new system of equations reads

$$\boldsymbol{k} + \boldsymbol{r} = \boldsymbol{B}\boldsymbol{x}' \tag{28}$$

and can be solved by least-squares as

$$\boldsymbol{x'} = \left(\boldsymbol{B^T P B}\right)^{-1} \boldsymbol{B^T P k} \tag{29}$$

where $\boldsymbol{P}$ is the weight matrix of the equation system. This permits to obtain in the first unknown $\boldsymbol{x'}(1)$ the correction to the initial approximate distance in terms of the approximate coordinates used for the receivers, dD_{ij}, as well as the corresponding precision in the first element of the covariance matrix, $\boldsymbol{C}_{\boldsymbol{x'}}(1,1)$, which is obtained as

$$\boldsymbol{C}_{\boldsymbol{x'}} = \hat{\sigma}_0^2 \left(\boldsymbol{B^T P B}\right)^{-1} \tag{30}$$

where $\hat{\sigma}_0^2$ is the variance of unit weight.

We briefly enumerate now the necessary ingredients to use this model for the determination of the distance of a single baseline with two high-grade geodetic receivers and two high-grade geodetic antennas (preferably of the same model, of choke-ring type):

- GNSS observation files (for one of the subsequent ingredients we assume them to be in RINEX format).
- Precise satellite ephemerides and clocks (SP3 files as provided by the IGS).
- ANTEX files as provided by the IGS for satellite antenna PCOs and variations, and ANTEX files for individual antenna calibrations for each of the stations.
- Results from the CSRS-PPP processing: mainly the approximate coordinates for both stations i and j, but also the estimated clock offsets for both stations i and j. Although receiver clock offsets are said to be completely cancelled in the double differences model, some receiver clocks may have so large offsets that the computation of satellite positions using so incorrect reception times may be significantly damaged unless at least approximate clock corrections are used (and for the sake of consistency we prefer to use here CSRS-PPP receiver clock offsets). Other estimates from the CSRS-PPP processing and their corresponding uncertainties are suggested to be used as indicated in the following subsections: tropospheric delays as well as L_1 and L_2 residuals.

Regarding the GNSS observation duration, the *Good practice guide for high accuracy global navigation satellite system based distance metrology* [9] indicates a minimum of 2 h, although better results can clearly be obtained with longer times: in [11] we suggested 10 h for a precise estimation of the distance, which is a similar result to that obtained by other researchers for the case of coordinate determination [21], and even better results are expected for observations spanning 24 h (where the residual periodic effects can be averaged out) or several days, such as in [22]. Also in agreement with the *Good practice guide* we prefer the use of L_1 carrier phase observations, provided the influence of the ionosphere in the double-differenced equations can be neglected or eliminated with sufficient accuracy (see the later section devoted to the ionospheric delay).

In what follows, we present a scheme for uncertainty propagation from the zero-differenced observations to the double-differenced observations (where we will note different particularities for the different error sources) and then from the double-differenced observations to the final estimation of the baseline length.

2.2. Uncertainty propagation

The error sources affecting positioning (and in our case, the determination of the baseline length) typically occur in the receiver-to-satellite line, that is, in the level of zero differences. However, the method developed is based on double differences, so that we need to estimate the errors in the zero differences, first, and then compute their propagation to the particular double-differenced equation. Then the propagation from the system of double-differenced equations to the final distance will be computed.

Let us note, first, that the uncertainty propagation of an error source from zero differences, say e_j^l, e_j^k, e_i^l and e_i^k, to double differences, say e_{ij}^{kl}, may take two different forms depending on whether in the error type e there is a zenith error to be mapped to the receiver-to-satellite direction by a suitable mapping function, which is the case of the tropospheric and ionospheric delays (although with usually different mapping function types), or whether the mapping function and the zenith error concepts do not apply for the error at hand, which is the case of the multipath effect and the antenna PCO and variations.

In the first case, where there is a zenith error above the station, say e_i and e_j for stations i and j, respectively, and a suitable mapping function for the receiver-to-satellite direction we can write

$$e_j^l = m_j^l e_j \tag{31}$$

$$e_i^l = m_i^l e_i \tag{32}$$

$$e_j^k = m_j^k e_j \tag{33}$$

$$e_i^k = m_i^k e_i \tag{34}$$

where m_j^l, m_j^k, m_i^l and m_i^k represent the application of the particular mapping function to the directions between stations i and j and satellites k and l and e is the error (tropospheric o ionospheric delay) that has to be corrected in the observation equation.

Let us denote by $\sigma_{e_j^l}$, $\sigma_{e_j^k}$, $\sigma_{e_i^l}$ and $\sigma_{e_i^k}$ the corresponding uncertainties of the errors e_j^l, e_j^k, e_i^l and e_i^k, which can be obtained as

$$\sigma_{e_j^l} = m_j^l \sigma_{e_j} \tag{35}$$

$$\sigma_{e_i^l} = m_i^l \sigma_{e_i} \tag{36}$$

$$\sigma_{e_j^k} = m_j^k \sigma_{e_j} \tag{37}$$

$$\sigma_{e_i^k} = m_i^k \sigma_{e_i} \tag{38}$$

where we have denoted by σ_{e_j} and σ_{e_i} the corresponding uncertainties of the zenith errors e_j and e_i provided they can be estimated from a reliable procedure (see the following sections) and where the mapping functions are assumed to have a completely negligible error for the purpose of uncertainty propagation.

Applying the law of covariance propagation to equations (31)–(34) we obtain

$$\sigma_{e_j^l e_i^l} = m_j^l m_i^l \sigma_{e_{ji}} \tag{39}$$

$$\sigma_{e_j^k e_i^k} = m_j^k m_i^k \sigma_{e_{ji}} \tag{40}$$

$$\sigma_{e_j^l e_i^k} = m_j^l m_i^k \sigma_{e_{ji}} \tag{41}$$

$$\sigma_{e_j^k e_i^l} = m_j^k m_i^l \sigma_{e_{ji}} \tag{42}$$

$$\sigma_{e_j^l e_j^k} = m_j^l m_j^k {\sigma_{e_j}}^2 \tag{43}$$

$$\sigma_{e_i^l e_i^k} = m_i^l m_i^k {\sigma_{e_i}}^2 \tag{44}$$

in terms of the variances and covariance of the zenith errors in j and i, ${\sigma_{e_j}}^2$, ${\sigma_{e_i}}^2$ and $\sigma_{e_{ji}}$, respectively.

Now let us consider the double difference

$$e_{ij}^{kl} = e_j^l - e_j^k - e_i^l + e_i^k. \tag{45}$$

The law of error propagation yields

$$\begin{aligned}{\sigma_{e_{ij}^{kl}}}^2 = {\sigma_{e_j^l}}^2 + {\sigma_{e_j^k}}^2 + {\sigma_{e_i^l}}^2 + {\sigma_{e_i^k}}^2 - 2\sigma_{e_j^l e_j^k} - 2\sigma_{e_j^l e_i^l} + 2\sigma_{e_j^l e_i^k} \\ + 2\sigma_{e_j^k e_i^l} - 2\sigma_{e_j^k e_i^k} - 2\sigma_{e_i^l e_i^k}\end{aligned} \tag{46}$$

and using the expressions in equations (35)–(44)

$$\begin{aligned}{\sigma_{e_{ij}^{kl}}}^2 = \left(m_j^{l2} + m_j^{k2}\right){\sigma_{e_j}}^2 + \left(m_i^{l2} + m_i^{k2}\right){\sigma_{e_i}}^2 - 2m_j^l m_j^k {\sigma_{e_j}}^2 \\ - 2m_j^l m_i^l \sigma_{e_{ji}} + 2m_j^l m_i^k \sigma_{e_{ji}} + 2m_j^k m_i^l \sigma_{e_{ji}} - 2m_j^k m_i^k \sigma_{e_{ji}} \\ - 2m_i^l m_i^k {\sigma_{e_i}}^2.\end{aligned} \tag{47}$$

Grouping common factors (note the dependence on $\sigma_{e_{ji}}$ disappears) we can write

$${\sigma_{e_{ij}^{kl}}}^2 = \left(m_j^l - m_j^k\right)^2 {\sigma_{e_j}}^2 + \left(m_i^l - m_i^k\right)^2 {\sigma_{e_i}}^2. \tag{48}$$

For the purpose of uncertainty estimation in baselines of up to few km (that is, station i relatively close to station j, thus very similar apparent receiver-to-satellite elevations) one can also consider $m_j^l = m_i^l$ and $m_j^k = m_i^k$, and write

$${\sigma_{e_{ij}^{kl}}}^2 = \left(m_j^l - m_j^k\right)^2 \left({\sigma_{e_j}}^2 + {\sigma_{e_i}}^2\right). \tag{49}$$

This means that the geometry of the particular double difference (given here by the squared difference between m_j^l and m_j^k) is the main factor defining the uncertainty in the double-differenced error: in some cases (for very similar elevations) the double-differenced error will be virtually zero whereas in others the sum of zenith errors at i and j will be considerably amplified by the squared difference between mapping functions.

Now let us examine the case where the type of error cannot be described by a zenith error and a mapping function, such as in the cases of multipath effect as well as antenna phase center and variations. For these cases equations (31)–(44) do not hold. Now, the uncertainties $\sigma_{e_j^l}$, $\sigma_{e_j^k}$, $\sigma_{e_i^l}$ and $\sigma_{e_i^k}$ need to be obtained by an appropriate procedure (see the subsequent sections devoted to modelling the multipath effect and the antenna errors) as well as the six covariances in equation (46).

The four covariances involving different stations (thus different multipath models or antenna calibrations), $\sigma_{e_j^l e_i^l}$, $\sigma_{e_j^k e_i^k}$, $\sigma_{e_j^l e_i^k}$, and $\sigma_{e_j^k e_i^l}$, can be regarded as zero. For the other two covariances we resort to the definition of the correlation coefficient ρ which permits us to write

$$\sigma_{e_j^l e_j^k} = \rho_{e_j^l e_j^k} \sigma_{e_j^l} \sigma_{e_j^k} \tag{50}$$

$$\sigma_{e_i^l e_i^k} = \rho_{e_i^l e_i^k} \sigma_{e_i^l} \sigma_{e_i^k}. \tag{51}$$

These correlation coefficients are unknown. We can either compute them from an available sample or simply assume them to have the value for the worst case (+1 or −1). With this latter assumption, the law of error propagation equation (46) results in

$${\sigma_{e_{ij}^{kl}}}^2 = {\sigma_{e_j^l}}^2 + {\sigma_{e_j^k}}^2 + {\sigma_{e_i^l}}^2 + {\sigma_{e_i^k}}^2 + 2\sigma_{e_j^l}\sigma_{e_j^k} + 2\sigma_{e_i^l}\sigma_{e_i^k} \tag{52}$$

or

$${\sigma_{e_{ij}^{kl}}}^2 = \left(\sigma_{e_j^l} + \sigma_{e_j^k}\right)^2 + \left(\sigma_{e_i^l} + \sigma_{e_i^k}\right)^2. \tag{53}$$

Having estimated the uncertainty in the double differences equations—either by equation (49) or equation (53) depending on whether a mapping function is in use or not for the particular error—we propagate these uncertainties to the final distance obtained after the least squares adjustment.

Defining

$$\boldsymbol{M} = \left(\boldsymbol{B}^{\mathrm{T}}\boldsymbol{P}\boldsymbol{B}\right)^{-1}\boldsymbol{B}^{\mathrm{T}}\boldsymbol{P} \tag{54}$$

we can write the solution vector, equation (29), as

$$\boldsymbol{x}' = \boldsymbol{M}\boldsymbol{k} \tag{55}$$

the effect of the uncertainties in the double differences equations used ${\sigma_{e_{ij}^{kl}}}^2$, ${\sigma_{e_{ij}^{km}}}^2 \ldots$ onto the final distance can be obtained by the law of covariance matrix propagation as

$$\boldsymbol{C}_{\boldsymbol{x}'} = \boldsymbol{M}\boldsymbol{C}_{\boldsymbol{k}}\boldsymbol{M}^{\mathrm{T}} \tag{56}$$

where

$$\boldsymbol{C}_{\boldsymbol{k}} = \begin{pmatrix} {\sigma_{e_{ij}^{kl}}}^2 & & \\ & {\sigma_{e_{ij}^{km}}}^2 & \\ & & \ldots \end{pmatrix} \tag{57}$$

and

$$\sigma_{D_{ij}} = \sqrt{\boldsymbol{C}_{\boldsymbol{x}'}(1,1)} \tag{58}$$

is the estimated uncertainty in the final distance due to the propagated uncertainties of the particular error source.

Now we have a look at the particular instances of application of these formulas for the existing relevant errors in the determination of distances up to 5 km in (possibly) non-horizontal baselines by double-differenced carrier phase observations.

2.3. Tropospheric delay

For horizontal short baseline distances the tropospheric delays cancel out in the double differences. This condition was assumed in our initial presentation of the GBDM technique [16] but it may no longer hold for our current problem of baselines up to 5 km with possibly significant height differences (tens or even hundreds of meters). In what follows, we present our strategy to correct the tropospheric delays and propagate the uncertainty of the correction to the final distance.

In short, the tropospheric delay corrections, T_{ij}^{kl}, are subtracted in the left-hand side of the model in equation (11) with the values provided by the CSRS-PPP service and then the corresponding uncertainties also provided by the CSRS-PPP are used to analyze the uncertainties in the double differences, first, and then in the final estimation of the baseline distance.

Note that, alternatively, we could use the values of the tropospheric delay corrections (instead of their uncertainties) as input in the equations of propagation to obtain not the propagated uncertainty but the approximate effect on the final distance of neglecting such tropospheric delay corrections. We highlight that this possible use is an approximation only, since the law of (random) error propagation rigorously applies to uncertainty propagation but not to systematic error propagation, where the errors have a definite size and sign. All in all, the result can give an overall indication of the impact on the final distance that entails neglecting the correction.

Referring now to the propagation of uncertainties in the tropospheric delay corrections, they are given by the CSRS-PPP service (at a level of confidence of 95%, $k = 2$) for the zenith directions, that is σ_{e_j} and σ_{e_i} for stations j and i, respectively. They need to be mapped to each receiver-to-satellite line of sight by the corresponding mapping functions.

Different mapping functions have been proposed in the last decades, ranging from very simple functions such as Black and Eisner's mapping [23]

$$m_j^l = \frac{1.001}{\sqrt{0.002001 + \sin^2 E_j^l}} \tag{59}$$

where E_j^l is the elevation of satellite l as seen from receiver j, to more elaborate and accurate functions such as Niell mapping function (NMF) [24], Vienna mapping function 1 (VMF1) [25], or the Global Mapping Function [26]. The use of NMF, VMF1 and GMF yield differences of the order of millimeters in the computation of the tropospheric delays but provide completely negligible differences when used to compute the double differenced tropospheric delays, while for the purpose of computing the uncertainty propagation to this double differences it is sufficient to use the simple Black and Eisner's formula.

In the application section we will study the impact on the final distance of disregarding the double-differenced tropospheric delay and also, for the case where double-differenced tropospheric delays are corrected, what is the rigorously propagated uncertainty from the uncertainties in the tropospheric delay corrections to the double-differenced corrections, first, and then to the final distance.

2.4. Ionospheric delay

While in the initial presentation of the GBDM technique [16] we assumed that the double-differenced ionospheric delays cancelled out due to the short length of the baselines (1 km at the most), this assumption may no longer hold for our current problem of baselines up to 5 km.

The best approach would be to use ionospheric delay corrections for the observations from each station along with their estimated uncertainties in a similar way to the case of the tropospheric delays. In its current version (version 3), however, the CSRS-PPP service is estimating these ionospheric delays in the GNSS processing although they are not being distributed to the users. The CSRS-PPP may possibly add this output in short as part of its version 4 to be released in 2022 (Banville 2021, personal communication). This would permit to use a consistent set of estimates (coordinates, clocks, observation residuals, tropospheric corrections and ionospheric corrections) for the GNSS-based distance determination.

Meanwhile, the best possibility seems to use a combination of L_1 and L_2 GPS carrier phases (or E_1 and E_{5a} for Galileo) that eliminates the ionospheric delay to the first order, such as the one known as L_3 by the group in Berna [27]

$$\varphi_3 = 77\varphi_1 - 60\varphi_2 \tag{60}$$

where φ_1, φ_2 and φ_3 are the carrier phases in unit cycles of L_1, L_2 and L_3, respectively, or, equivalently

$$\Phi_3 = \frac{{f_1}^2}{{f_1}^2 - {f_2}^2}\Phi_1 - \frac{{f_2}^2}{{f_1}^2 - {f_2}^2}\Phi_2 \tag{61}$$

where Φ_1, Φ_2 and Φ_3 are the carrier phases in meters for L_1, L_2 and L_3, respectively, and f_1 and f_2 are the carrier frequencies of L_1 and L_2.

Although these combinations of L_1 and L_2 (or E_1 ans E_{5a}) are indeed quasi ionosphere-free, the existing residual error is completely eliminated in the double differences (with a completely negligible uncertainty). Obviously, a combination of three frequencies can also be used. The cost, both for the dual frequency combination and, even more so, for the triple frequency, is an increase in noise compared to the use of L_1 (by a factor of approximately 3 for the case of L_3 [27, p 53]).

Another possibility is the use of the Klobuchar model. Although the Klobuchar model is estimated to be able to correct no more than about 50% of the delay at zero differences,

the computation of double differences largely cancels out the residual error and does not have a significant effect on the final distance.

2.5. Multipath effect

As acknowledged in the *Good practice guide* [9] a careful observation site selection (when possible) plus the use of choke-ring antennas and long observation times are the best advice to minimize the multipath effect. Going beyond this advice, now at the computational level, is difficult.

In particular, obtaining a reliable estimation for the multipath error affecting every observation (along with an uncertainty for this estimation) is a daunting task.

For the case of GPS observations, however, we can use the sidereal filtering technique provided observations in different days are available thanks to the apparent repeating period of the GPS constellation of one sidereal day. For other constellations this is not practical due to their longer apparent repeating periods.

As explained in [16], the sidereal filtering technique assumes that all significant sources of error have been taken into account so that the observation residuals (in our case the residuals obtained after the CSRS-PPP processing) contain mostly multipath. For every observing site and every satellite, we can match the observation residuals of different consecutive sidereal days and construct a time-varying multipath model valid for the particular observation site and satellite. The matching of residuals is better done by using the closest azimuth and elevation values of the satellite between days or, secondly preferred (because the repeating period slightly deviates from one sidereal day in a different way for every satellite) by shifting the residuals of the satellite one sidereal day. It is advisable to have three or more observing days.

The model constructed from the matched residuals (as in [16, figure 5]) not only provides the value of the multipath correction (the average values) but also an estimate of its uncertainty (the experimental dispersion).

Beyond the restriction of use of this technique to GPS observations, it has to be acknowledged that the decimation of observations to 30 s performed by the CSRS-PPP significantly hampers the application of the sidereal filtering technique, enabling only a poor satellite matching from 30 s observation rates instead of the more accurate definition that would be obtained, e.g. using 1 s observation rates. Any alternative computation of the sample of residuals, by a user-developed software for example, would be disadvantageous, however, by breaking the consistency in the set of auxiliary estimates used (coordinates, clocks, observation residuals, tropospheric corrections and ionospheric corrections all derived from CSRS-PPP).

2.6. Antenna calibration

The point where the signal is received in the antenna is not a fixed point that can be mechanically identified, but varies with the frequency, azimuth and elevation of the incoming signal. To refer the measurement to the antenna reference point (which is externally accessible to the user) a PCO, taken as a mean value for the entire range of satellite azimuth and elevations, plus an additional PCV, dependent on the particular azimuth and elevation of the receiver-to-satellite line of sight, are needed. These are given for each signal frequency in GNSS antenna calibrations files—using the ANTEX format—which may originate from a general calibration or from an individual calibration of the particular antenna by a dedicated procedure.

The IGS calibration tables are the standard calibration files of general type. They offer mean calibration values for each type of antenna (PCOs and tabulated PCVs in terms of azimuth and elevation, for each signal frequency) after the calibration of different antennas of the same model. Individual calibration tables, on the contrary, are obtained by a dedicated method (robot calibration or anechoic chamber) to individually characterize the particular antenna.

Recently, some authors have presented special methods for quantifying the errors, validating and comparing GNSS antenna calibrations [28, 29]. To determine the baseline distance along with its corresponding uncertainty propagated from the original error sources, we need to estimate and incorporate into the uncertainty budget the amount of uncertainty attributed to the antenna calibration in use. Since our GBDM+ methodology aims to develop for this purpose simple methods using standard products and solutions, where possible, we propose to compare the values from the individual robot calibration versus those from the individual anechoic chamber calibration (as they are the leading methods for antenna calibration), provided they are both available for the antenna in use, or, alternatively, any available individual calibration versus the generic calibration, so that the difference between both calibrations will be taken as the uncertainty ($k = 1$) of the individual calibration correction.

These uncertainties at the level of zero differences will be then propagated to double differences, equation (53), and then to the baseline distance, equations (56)–(58).

2.7. Instrument setup

The instrument setup must be prepared following the same scheme, in particular with antennas oriented towards north, and with the same cable routing and mounting devices. As said before, the antennas must be of choke-ring type (preferably of the same model) and have been individually calibrated at least by one of the existing methods (chiefly, robot calibration and anechoic chamber).

While the uncertainty in the horizontal centering of the instrument can be neglected, the measurement of the antenna heights is especially critical. As it is acknowledged in the *Good practice guide* [9, p 13] the use of a folding tape or ruler is insufficient. As we will see in the application section, for high elevation differences between the baseline endpoints, it is possible that one third of the uncertainty in the antenna height determination propagates to uncertainty in the baseline distance.

We now propose a strategy to accurately measure the antenna height along with the corresponding uncertainty. The uncertainties in the determination of antenna heights in each

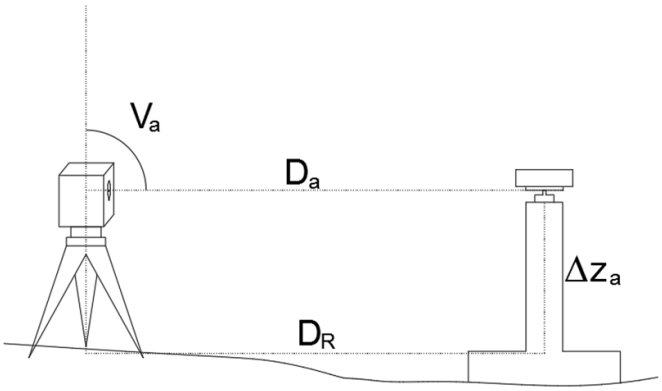

Figure 1. Vertical angle measurement to the bottom of antenna mount.

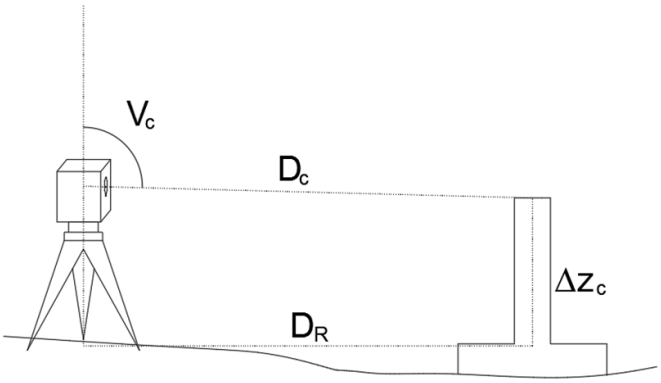

Figure 2. Vertical angle measurement to the top of pillar.

baseline endpoint will be then propagated to the final distance with the appropriate formulas. In what follows we assume the benchmark consists in a geodetic pillar, although the proposed procedure could be easily adapted to other cases of interest.

Let use a total station set up a few meters apart from the antenna so that the bottom of the antenna mount is as close as practically possible to the horizontal line of site, i.e. $V_\mathrm{a} \approx 100^\mathrm{g}$ (this is important to ensure that the vertical angle also corresponds to the vertical angle of the antenna mount at its vertical axis). Only the vertical angle V_a needs to be noted down, although in figure 1 the geometric (or slant) distance to the antenna D_a and the corresponding reduced (or horizontal) distance D_R are also indicated along with the increment of height from the total station ground point to the bottom of the antenna Δz_a.

Then the antenna is dismounted and the vertical angle to the top of the pillar at the centering point, V_c, is noted down, figure 2. To accurately measure this vertical angle it may be convenient to point to the right (and then left) external tangent of the centering device (if there is one, e.g. a $5/8''$ centering screw). As in the case of figure 1 we also show the geometric distance to the antenna D_c, the reduced distance D_R and the increment of height from the total station ground point Δz_c.

Finally, we setup a prism (corner cube reflector) on top of the pillar and measure the distance D_p, and the corresponding vertical angle V_p.

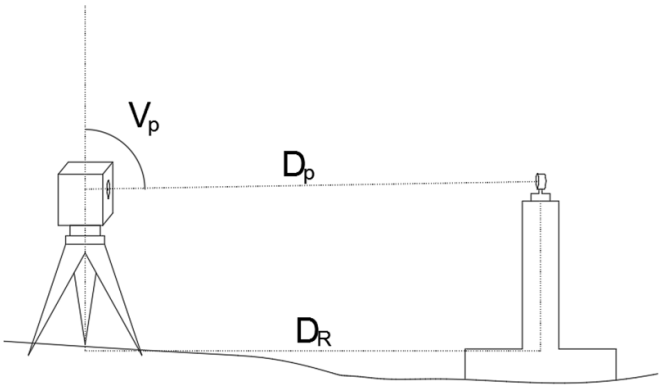

Figure 3. Vertical angle and distance measurement to a prism.

This final step permits us to calculate the reduced distance D_R as

$$D_\mathrm{R} = D_\mathrm{p} \sin V_\mathrm{p}. \tag{62}$$

This reduced distance is the same for the three schemes figures 1–3. Further, for figures 1 and 2 we can write, respectively

$$\Delta z_\mathrm{a} = \frac{D_\mathrm{R}}{\tan V_\mathrm{a}} \tag{63}$$

$$\Delta z_\mathrm{c} = \frac{D_\mathrm{R}}{\tan V_\mathrm{c}} \tag{64}$$

so that the antenna height over the centering mark on top of the pillar, h, can now be determined as

$$h = \Delta z_\mathrm{a} - \Delta z_\mathrm{c} \tag{65}$$

or

$$h = D_\mathrm{p} \sin V_\mathrm{p} \left(\frac{1}{\tan V_\mathrm{a}} - \frac{1}{\tan V_\mathrm{c}} \right). \tag{66}$$

The process can be repeated and done from other two or three sides.

We can apply the law of error propagation to compute the uncertainty in the antenna height, σ_h, in terms of the uncertainties in the measured values D_p, V_p, V_a and V_c, respectively, $\sigma_{D\mathrm{p}}$, $\sigma_{V\mathrm{p}}$, $\sigma_{V\mathrm{a}}$ and $\sigma_{V\mathrm{c}}$, as follows

$$\sigma_\mathrm{h}{}^2 = \left(\frac{\partial h}{\partial D_\mathrm{p}} \right)^2 \sigma_{D_\mathrm{p}}{}^2 + \left(\frac{\partial h}{\partial V_\mathrm{p}} \right)^2 \sigma_{V_\mathrm{p}}{}^2 + \left(\frac{\partial h}{\partial V_\mathrm{a}} \right)^2 \sigma_{V_\mathrm{a}}{}^2 + \left(\frac{\partial h}{\partial V_\mathrm{c}} \right)^2 \sigma_{V_\mathrm{c}}{}^2 \tag{67}$$

with

$$\frac{\partial h}{\partial D_\mathrm{p}} = \sin V_\mathrm{p} \left(\frac{1}{\tan V_\mathrm{a}} - \frac{1}{\tan V_\mathrm{c}} \right) \tag{68}$$

$$\frac{\partial h}{\partial V_\mathrm{p}} = D_\mathrm{p} \cos V_\mathrm{p} \left(\frac{1}{\tan V_\mathrm{a}} - \frac{1}{\tan V_\mathrm{c}} \right) \tag{69}$$

$$\frac{\partial h}{\partial V_a} = -D_p \sin V_p \frac{1}{\sin^2 V_a} \tag{70}$$

$$\frac{\partial h}{\partial V_c} = -D_p \sin V_p \frac{1}{\sin^2 V_c}. \tag{71}$$

Assuming the same uncertainty σ_V in the determination of all vertical angles, the expression for the uncertainty reduces to

$$\begin{aligned}\sigma_h{}^2 = \sin^2 V_p \left(\frac{1}{\tan V_a} - \frac{1}{\tan V_c}\right)^2 \sigma_{D_p}{}^2 + D_p{}^2 \\ \times \left[\cos^2 V_p \left(\frac{1}{\tan V_a} - \frac{1}{\tan V_c}\right)^2 \right. \\ \left. + \sin^2 V_p \left(\frac{1}{\sin^4 V_a} + \frac{1}{\sin^4 V_c}\right)\right] \sigma_V{}^2.\end{aligned} \tag{72}$$

Simplifications of this formula could be given with no significant loss of accuracy due to the proximity of all vertical angles to 100^g angles. In particular we can approximate all squared sines to 1 and the squared cosine to zero, which yields

$$\sigma_h{}^2 = \left(\frac{1}{\tan V_a} - \frac{1}{\tan V_c}\right)^2 \sigma_{D_p}{}^2 + 2 D_p{}^2 \sigma_V{}^2. \tag{73}$$

Since the uncertainties of the antenna heights in the baseline endpoints are very small quantities we can safely neglect the earth's curvature for the purpose of propagating these uncertainties to the baseline distance.

This geometric distance between the baseline endpoints, D_{ij}, is related to the reduced distance D_{Rij} and the increment of height between stations Δh_{ij}, neglecting the earth's curvature, by the expression

$$D_{ij} = \sqrt{D_{Rij}{}^2 + \Delta h_{ij}{}^2}. \tag{74}$$

The law of error propagation yields the expression for uncertainty in the geometric distance in terms of uncertainty in one height (say i)

$$\sigma_{D_{ij}} = \frac{\partial D_{ij}}{\partial \Delta h_{ij}} \sigma_{h_i} \tag{75}$$

$$\sigma_{D_{ij}} = \frac{\Delta h_{ij}}{D_{ij}} \sigma_{h_i}. \tag{76}$$

And taking into account the uncertainties in the antenna heights of both baseline endpoints, i and j, computed by making use of equation (73) in each endpoint, we can finally write

$$\sigma_{D_{ij}} = \frac{\Delta h_{ij}}{D_{ij}} \sqrt{\sigma_{h_i}{}^2 + \sigma_{h_j}{}^2}. \tag{77}$$

In section 3 we will obtain and discuss some numerical results after the application of these formulas.

2.8. Additional remarks

As it was explained in our initial presentation of the GBDM method [16], in the case of horizontal baselines of several hundred meters only and low multipath, a free-ambiguity approach could be used: in equation (11) ionospheric and tropospheric double-differenced delays, I_{ij}^{kl} and T_{ij}^{kl}, could be neglected and the smallness in coordinate corrections dX_j, dY_j, dZ_j after a PPP processing for obtaining the approximate coordinates entailed that the quantity $\varphi_{ij}^{kl} - \rho_{ij0}^{kl}/\lambda$ be close to an integer value, the ambiguity, and this ambiguity easily determined by rounding the quantity to its nearest integer thus avoiding the ambiguity determination by the usual more costly procedures.

For the case of baselines up to 5 km with a possibly significant height difference, however, we have experienced that the closeness to an integer value of the term $\varphi_{ij}^{kl} - \rho_{ij0}^{kl}/\lambda$ does not always happen, no matter how close to their exact values the approximate coordinates are, because of the effect of the remaining corrections (ionospheric and tropospheric delays, and multipath effect). Dubious values around half a cycle prevent one to safely adopt the rounding term approach in this case so that some kind of ambiguity determination by solving the system of observation equations has to be performed. Two different easy procedures, however, prove to have a high ambiguity success rate (by making both determinations an even higher degree of security is obtained for the coincident ambiguities):

- solving the system of equations to obtain floating ambiguities and then rounding them to their nearest integer.
- setting to zero the coordinate corrections $dX_j = 0$, $dY_j = 0$, and $dZ_j = 0$ in equation (10), which makes sense due to the accurate initial PPP processing, and obtaining ambiguities by solving the simplified system of equations: first as floating ambiguities and then rounded to their nearest integer.

Regarding the L_3 ambiguities, they can be obtained in terms of the L_1 ambiguities and the wide-lane combination ambiguities.

Finally, it is worth mentioning that the other sources of error of the GNSS systems not mentioned before are not relevant to our double differences approach, since they completely cancel out. This is the case, for example, of relativistic effects, which cancel for all practical purposes in relative positioning [30, p 229], and the windup effect ('completely cancelled in double differences' [31, p 731]).

Figure 4 summarizes the main steps of the GBDM+ methodology starting from the preliminary operations (individual antenna calibration), through the field measurements (GNSS observations and antenna height measurement) and external data collection, up to the PPP processing (with CSRS-PPP) and double differences processing to finally obtain the baseline distance along with its uncertainty (with in-house developed software). The in-house developed software, written under Matlab, was initially developed by the authors for [11, 12], refined later for [16] and now extended to incorporate the different issues presented in the current paper.

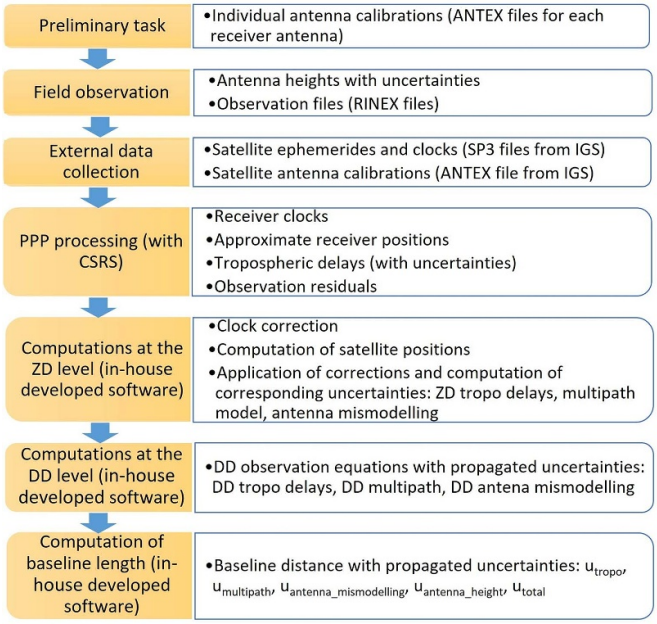

Figure 4. Scheme of the GDBM+ methodology.

3. Results and discussion

We apply the method to the case of *Cortes de Pallás* deformation monitoring network [5], figure 5, which was observed with the submillimetric Mekometer ME5000 EDM during daytime and GNSS during nighttime in the 21–23 July 2020 observation campaign. Two Leica GS10 GNSS multi-constellation receivers (GLONASS, GPS and Galileo) were used with two Leica AR25 multi-constellation individually calibrated choke-ring antennas (calibrated with the anechoic chamber method) during two nights observing 10 h each night, roughly from 19:00 to 5:00 UTC, with data every 1 s although only epochs every 30 s were used for the computation with an elevation mask of 15° (although the receivers tracked signals above 10°). The observation files are available in a public repository as indicated at the end of the paper. Precise ephemerides and clocks, of the 'final' type (igs2115_.sp3 files) were used for the computations. In particular, we analyze here the longest baseline of the network having a slant distance of almost 2 km and a substantial height difference of 350 m.

In [32] we show the detailed results of the last deformation monitoring observation campaign (the initial campaign was already presented in [5]), including the agreement within 1 mm between the GNSS-derived distance (from 10 h during each two nights) and the ME5000-derived distance. Here we present the complete results of the uncertainty propagation from zero differences to double differences, first, and then to the final baseline distance for the relevant sources of error in our GBDM+ method. As it has been repeatedly mentioned, this is the main contribution of the current paper, since it provides the user with the detailed analysis of the uncertainty in the different error sources and the propagation of these uncertainties through the particular double-differenced equations leading to the determination of the

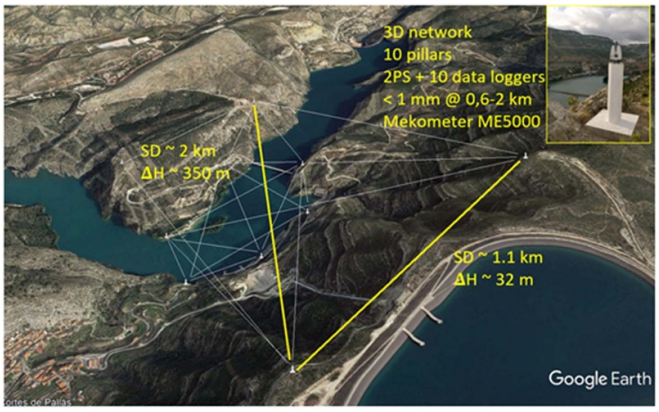

Figure 5. *Cortes de Pallás* deformation monitoring network.

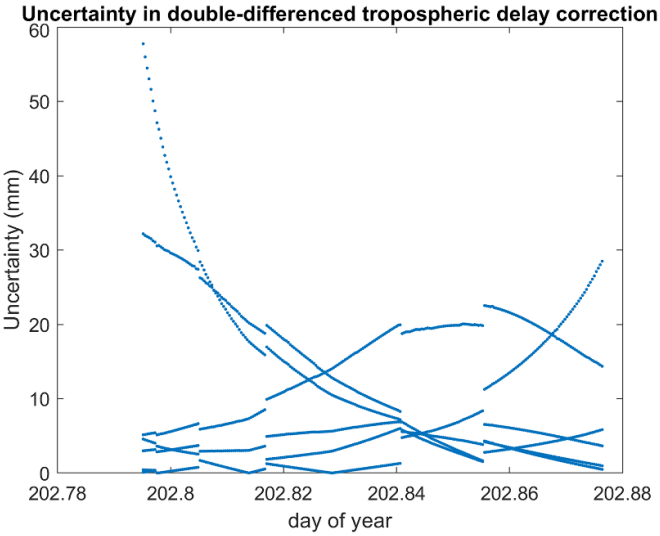

Figure 6. Uncertainty in the double differenced tropospheric delay correction (22 July 2020, 19:05:00–21:05:00 UTC).

baseline distance, whose final value can be now accompanied with the corresponding uncertainty budget. This study of uncertainty propagation, which is particular to the observables and equations by which the distance is finally determined, is not possible to be carried out by the existing software packages and constitutes the main advantage of the GBDM+ method enabling its use for metrological purposes.

Starting with the tropospheric delay, whose uncertainty can be obtained from CSRS-PPP files, the propagation to double differences equations by equation (49) results in the uncertainties shown in figure 6 for the first two observation hours.

Just as we reasoned right after equation (49), we can see that the geometry of the particular double difference dominates the resulting uncertainty and the assumption of a constant uncertainty value at the level of double differences would be really ill-advised: there are values of several cm while others are really close to zero. We can also guess from figure 6 the different combinations of satellites (satellite pairs) involved in the particular double differenced equation as well as the particular time instant where the reference satellite in the equation

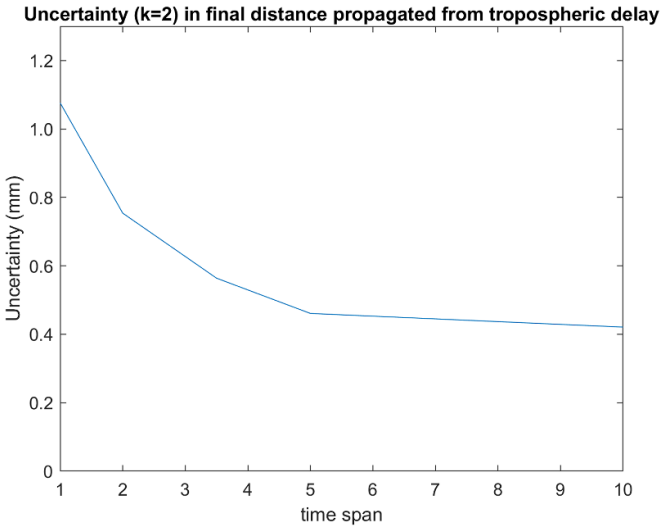

Figure 7. Uncertainty in the baseline distance propagated from the tropospheric delay uncertainty for different observation time spans (average values for all the different time blocks).

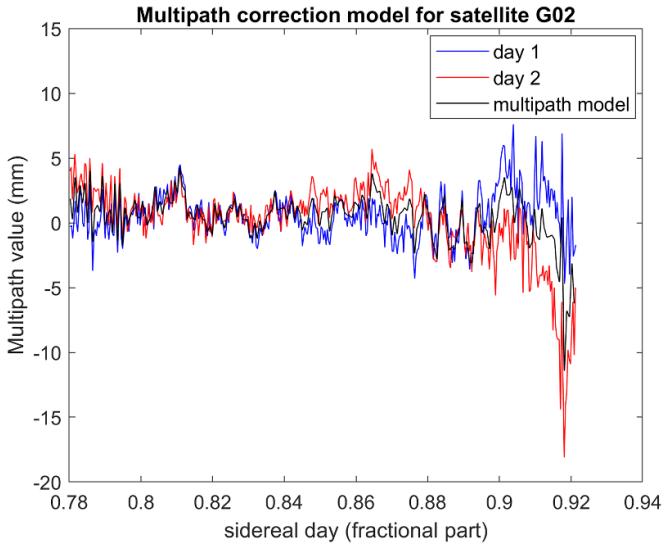

Figure 8. Multipath correction model for satellite G02.

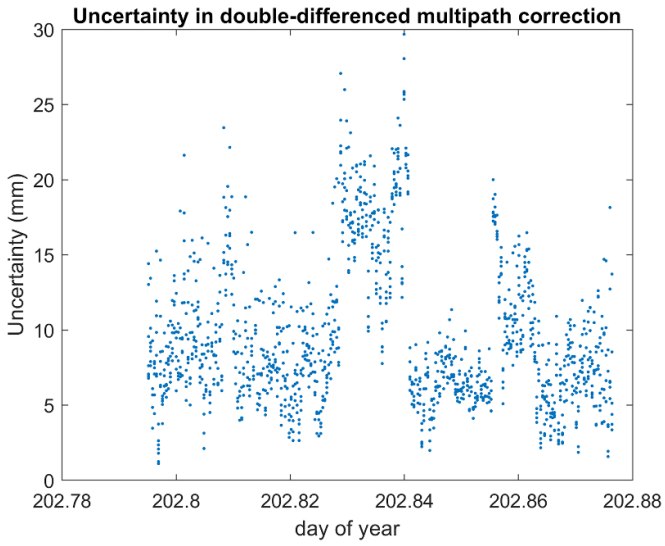

Figure 9. Uncertainty in the double differenced multipath correction (22 July 2020, 19:05:00–21:05:00 UTC).

is changed: in the particular moment of change of reference satellite, the double-differenced uncertainty experiences a jump explained by the change in uncertainty resulting by the change in one of the satellites of the pair (namely, the reference satellite, which has been taken as the one with highest elevation and usually has less uncertainty).

The propagation of these uncertainties in the double differences equations along the system of equations solution resulting in the final distance determination, equations (56)–(58), yields 0.0005 m using the observation time span in figure 6. Longer time spans yield lower uncertainties for the distance, as expected. This can be seen in figure 7, where the resulting uncertainties in the distance in terms of the observation time spans are given.

We want to emphasize that these results on the propagation of the uncertainty in tropospheric delay correction up to the final distance depend on the baseline studied, that is, its location, orientation, slope and distance, as well as on the moment of observation (observation time span, available observables…) That is, the conclusions drawn are particular to this experiment and cannot be extrapolated to other experiments.

Regarding the ionospheric delay, in the present case the differences between the computation with L_3 and L_1 corrected with Klobuchar model are negligible. As explained before, the corresponding uncertainty is taken as zero. Alternatively, in the future, if CSRS-PPP values for the ionospheric delay error are available along with their uncertainties, these will be corrected from the L_1 observation and the uncertainty of the correction propagated to the final result as in the previous case of the troposphere. Although of negligible magnitude, as expected, this result has its formal interest in the elaboration of the complete uncertainty budget.

With respect to the multipath effect, after constructing multipath correction models for the different satellites as explained in section 2.5, e.g. figure 8 for satellite G02, we can obtain the corresponding uncertainties in double differences by using equation (53), figure 9.

The propagation to the final distance, equations (56)–(58), gives 0.0004 m for the observation time span in figure 9. As expected, longer time spans yield lower uncertainties for the distance, figure 10.

Regarding antenna calibration uncertainties, we present here the results after estimating the uncertainty in the individual antenna calibrations available (realized with the anechoic chamber method by the IGG—Universität Bonn) by comparison with the generic IGS antenna calibration model. At the zero differences level there are discrepancies up to a few mm between the individual and the generic calibration. By use of equation (53), they lead to the uncertainties in double differenced values given in figure 11, where the change of

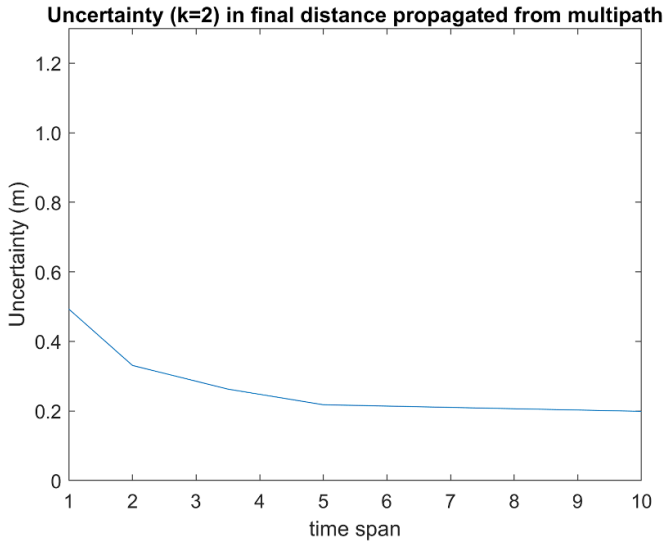

Figure 10. Uncertainty in the baseline distance propagated from the multipath uncertainty for different observation time spans (average values for all the different time blocks).

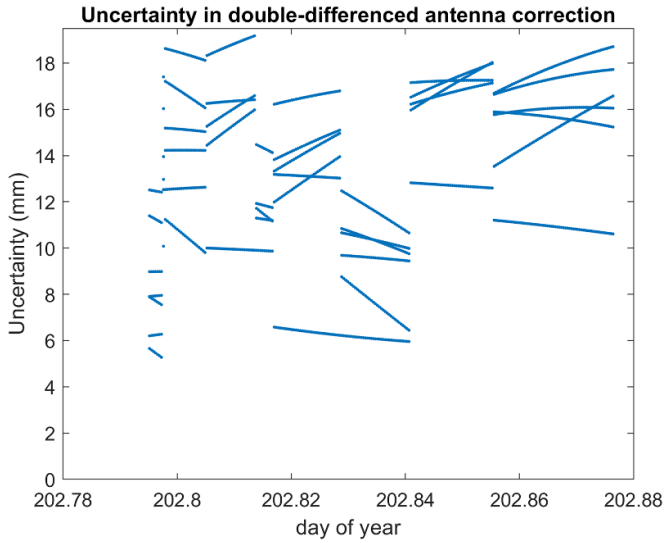

Figure 11. Uncertainty in the double differenced antenna calibration (22 July 2020, 19:05:00–21:05:00 UTC).

reference satellite in the formation of double differences is again evident.

The propagation to the final distance, computed by equations (56)–(58), gives 0.0005 m for the observation time span in figure 11. As expected, longer time spans yield lower uncertainties for the distance, as it can be seen in figure 12.

With respect to the instrument setup, we give figures for the application of equations (66)–(77) to the determination of the antenna height with a Leica TM30 Total Station although at the campaign the antenna height was simply determined by the inaccurate use of a folder tape. Assuming $V_a = 99.9550^g$,

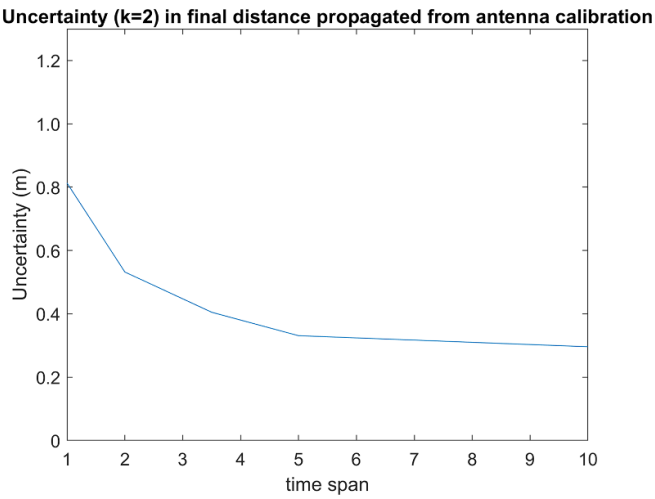

Figure 12. Uncertainty in the baseline distance propagated from the antenna calibration uncertainty for different observation time spans (average values for all the different time blocks).

Table 1. Total uncertainty budget in the baseline distance propagated from all error sources, $k = 2$, values in mm (average values for all the different time blocks).

Observ. time span (h)	$u_{\text{tropo.delay}}$	$u_{\text{multipath}}$	$u_{\text{antenna model}}$	$u_{\text{antenna heights}}$	u_{total}
1	1.08	0.49	0.81	0.03	1.44
2	0.75	0.33	0.53	0.03	0.98
3.5	0.56	0.26	0.40	0.03	0.74
5	0.46	0.22	0.33	0.03	0.61
10	0.42	0.20	0.30	0.03	0.55

$V_c = 101.0962^g$, $V_p = 99.9220^g$ and $D_p = 5.126$ m, the antenna height results in $h = 0.0919$ m. The technical specifications give $\sigma_V = 0.0003^g$, which we could increase to $\sigma_V = 0.0010^g$ to account for possible pointing inaccuracies at these short distances, and $\sigma_D = 0.0006$ m in precise mode, which we could increase to $\sigma_D = 0.0010$ m (or even 0.0020 m, it does not have a significant impact on the result) to account for the possible inexactness in the centering of the prism mount. The resulting accuracy is $\sigma_h = 0.00011$ m for the determination of one antenna height, which in this simulation we can assume equal in both baseline endpoints: $\sigma_{hi} = \sigma_{hj} = 0.00011$ m. By using equation (77) it is obtained $\sigma_{Dij} = 0.00003$ m for an the approximate height difference and baseline distance of 350 and 1916 m, respectively.

The total uncertainty budget for $k = 2$ (95% level of confidence) is given in table 1. As it can be seen, the uncertainty in the tropospheric delay has the main in the current case of study where there is a considerable height difference, but this could obviously be different for other cases of application. Figure 13 shows the final uncertainty in terms of the observation time span.

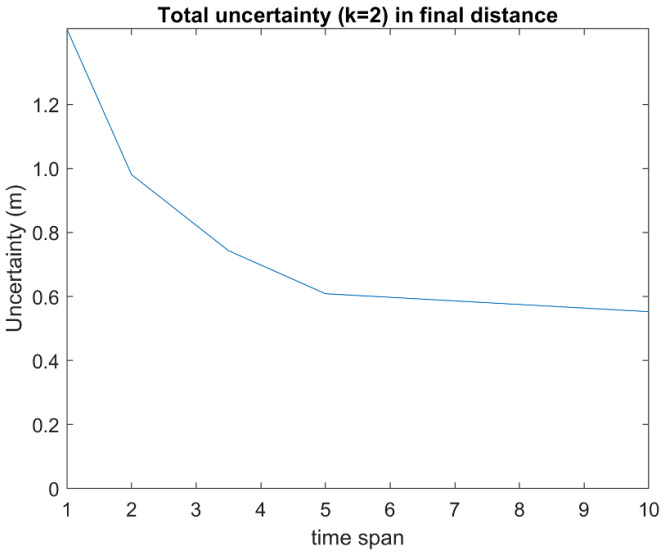

Figure 13. Total uncertainty in the baseline distance propagated from all error sources (average values for all the different time blocks).

4. Conclusions and future work

We have proposed a methodology for an improved GBDM for use in baselines of up to 5 km with a possibly significant height difference between baseline endpoints. The uncertainty in the correction of the different sources of error has been estimated and rigorously propagated throughout the double-difference equations of the system of equations until the corresponding uncertainty in the final baseline distance.

The results obtained are particular to the concerned baseline and observations and cannot be extrapolated to other experiments.

The proposed methodology has been applied to an example from a deformation monitoring network. The uncertainties in the contributing error sources were reliably estimated, first, and then propagated to the double differences equations and the final baseline length. For this example, where the height difference between baseline ends was significant (around 350 m in the 2 km baseline), the uncertainty in the tropospheric delay was the dominant contribution to the uncertainty in the final length, with a value of 1.1 mm. The uncertainties stemming from the antenna model, multipath effect and antenna height determination (by the method proposed) followed in order of importance, with values of 0.8, 0.5 and below 0.1 mm, respectively.

This methodology is being applied in a near future to the campaigns at the EURO5000 calibration baseline and the CERN geodetic network and compared therein with the results from the new two-color EDM prototypes that are being developed in the ongoing Geometre project.

Data availability statement

The data that support the findings of this study are openly available at the following URL/DOI: https://doi.org/10.5281/zenodo.6566948 [33].

Acknowledgments

The work leading to this paper was performed within the 18SIB01 GeoMetre project of the European Metrology Programme for Innovation and Research (EMPIR). This project has received funding from the EMPIR programme co-financed by the Participating States and from the European Union's Horizon 2020 research and innovation programme, funder ID: 10.13039/100014132. Raquel Luján acknowledges the funding from the *Programa de Ayudas de Investigación y Desarrollo (PAID-01-20) de la Universitat Politècnica de València.*

ORCID iDs

Sergio Baselga https://orcid.org/0000-0002-0492-4003
Luis García-Asenjo https://orcid.org/0000-0001-6535-2216
Pascual Garrigues https://orcid.org/0000-0003-2631-1889
Raquel Luján https://orcid.org/0000-0002-6300-0409

References

[1] Bureau International des Poids et Mesures 2019 *The International System of Units (SI)* 9th edn (Sèvres: BIPM)
[2] Pollinger F *et al* 2016 JRP SIB60 metrology for long distance surveying–a concise survey on major project results *3rd Joint Int. Symp. on Deformation Monitoring (JISDM)* (*Vienna, Austria, 30 March–1 April*) (https://doi.org/10.1364/OE.24.024092)
[3] European Organization for Nuclear Research 2016 Technical Description for high precision geodetic metrology at CERN, market survey EDMS No.: 1609015, MS-4192/EN (Meyrin: CERN)
[4] Jokela J and Häkli P 2010 *Interference Measurements of the Nummela Standard Baseline in 2005 and 2007* (Helsinki: Finnish Geodetic Institute)
[5] García-Asenjo L, Martínez L, Baselga S and Garrigues P 2019 Establishment of a multi-purpose 3D geodetic reference frame for deformation monitoring in Cortes de Pallás (Spain) *4th Joint Int. Symp. on Deformation Monitoring (JISDM)* (Athens, Greece, *15–17 May*)
[6] Pollinger F *et al* 2021 Large-scale dimensional metrology for geodesy—first results from the European GeoMetre project *Scientific Assembly of the Int. Association of Geodesy (IAG)* (*Beijing, China, 28 June–2 July*)
[7] Collilieux X, Métivier L, Altamimi Z, van Dam T and Ray J 2011 Quality assessment of GPS reprocessed terrestrial reference frame *GPS Solut.* **15** 219–31
[8] Altamimi A, Rebischung P, Métivier L and Collilieux X 2016 ITRF2014: a new release of the international terrestrial reference frame modeling nonlinear station motions *J. Geophys. Res.* **121** 6109–31
[9] Bauch A *et al* 2017 *Good Practice Guide for High Accuracy Global Navigation Satellite System Based Distance Metrology* Revised Version 2 (Braunschweig: JRP SIB60 Surveying Consortium)
[10] Pollinger F *et al* 2022 The European GeoMetre project—developing enhanced large-scale dimensional metrology for geodesy *5th Joint Int. Symp. on Deformation Monitoring (JISDM)* (*Valencia, Spain, 20–22 June*)
[11] Baselga S, García-Asenjo L and Garrigues P 2013 Submillimetric GPS distance measurement over short baselines: case study in inner consistency *Meas. Sci. Technol.* **24** 075001

[12] Baselga S, García-Asenjo L and Garrigues P 2014 Submillimetric GPS distance measurement over short baselines: noise mitigation by global robust estimation *Meas. Sci. Technol.* **25** 105004
[13] Koivula H, Häkli P, Jokela J, Buga A and Putrimas R 2012 GPS metrology—bringing traceable scale to local crustal deformation GPS network *Proc. 2009 IAG Symp.* vol 136, ed S Kenyon, M Pacino and U Marti (*Buenos Aires, Argentina*, *31 August–4 September 2009*) (International Association of Geodesy Symposia) pp 105–12
[14] García-Asenjo L, Atkins C, Baselga S, Ziebart M, Garrigues P and Luján R 2017 Submillimetric GNSS distance determination with multipath mitigation *6th Int. Coll. on Scientific and Fundamental Aspects of GNSS/Galileo* (*Valencia, Spain*, *25–27 October*)
[15] Špánik P, García-Asenjo L and Baselga S 2019 Optimal combination and reference functions of signal-to-noise measurements for GNSS multipath detection *Meas. Sci. Technol.* **30** 044001
[16] García-Asenjo L, Baselga S, Atkins C and Garrigues P 2021 Development of a submillimetric GNSS-based distance meter for length metrology *Sensors* **21** 1145
[17] Banville S, Hassen E, Lamothe P, Farinaccio J, Donahue B, Mireault Y, Goudarzi M A, Collins P, Ghoddousi-Fard R and Kamali O 2021 Enabling ambiguity resolution in CSRS-PPP *Navigation* **68** 433–51
[18] Atiz O M and Kalayci I 2021 Performance assessment of PPP-AR positioning and zenith total delay estimation with modernized CSRS-PPP *Artif. Satell.* **56** 18–34
[19] Mendez-Astudillo J, Lau L, Tang Y-T and Moore T 2018 Analysing the zenith tropospheric delay estimates in on-line precise point positioning (PPP) services and PPP software packages *Sensors* **18** 580
[20] Meyer T H 2010 *Introduction to Geometrical and Physical Geodesy: Foundations of Geomatics* (Redlands: ESRI Press)
[21] Hughes J C, Banks J A, Kerkhoff A J, Tolman B W and Wyant J R 2006 Sub-millimeter precision GPS survey system at the Holloman high speed test track *19th Int. Technical Meeting of the Satellite Division of the Institute of Navigation (ION GNSS 2006)* (*Fort Worth, Texas*, *26–29 September*)
[22] Wezka K, García-Asenjo L, Próchniewicz D, Baselga S, Szpunar R, Garrigues P, Walo J and Luján R 2022 EDM-GNSS distance comparison at the EURO5000 calibration baseline: preliminary results *5th Joint Int. Symp. on Deformation Monitoring (JISDM)* (*Valencia, Spain*, *20–22 June*)
[23] Black H D and Eisner A 1984 Correcting satellite Doppler data for tropospheric effects *J. Geophys. Res.* **89** 2616–26
[24] Niell A E 1996 Global mapping functions for the atmosphere delay at radio wavelengths *J. Geophys. Res.* **101** 3227–46
[25] Boehm J, Werl B and Schuh H 2006 Troposphere mapping functions for GPS and very long baseline interferometry from European Centre for medium-range weather forecasts operational analysis data *J. Geophys. Res.* **111** B02406
[26] Boehm J, Niell A, Tregoning P and Schuh H 2006 Global mapping function (GMF): a new empirical mapping function based on numerical weather model data *Geophys. Res. Lett.* **33** L07304
[27] Dach R, Lutz S, Walser P and Fridez P (eds) 2015 *Bernese GNSS Software Version 5.2. User Manual* (Bern: Bern Open Publishing)
[28] Kallio U, Koivula H, Lahtinen S, Nikkonen V and Poutanen M 2019 Validating and comparing GNSS antenna calibrations *J. Geod.* **93** 1–18
[29] Bergstrand S, Jarlemark P and Herbertsson M 2020 Quantifying errors in GNSS antenna calibrations: towards *in situ* phase center corrections *J. Geod.* **94** 105
[30] Leick A, Rapoport L and Tatarnikov D 2015 *GPS Satellite Surveying* 4th edn (Hoboken, NJ: Willey)
[31] Teunissen P J G and Montenbruck O (eds) 2017 *Springer Handbook of Global Navigation Satellite Systems* (Cham: Springer)
[32] García-Asenjo L, Martínez L, Baselga S, Garrigues P and Luján R 2022 Geodetic monitoring of a high-precision reference frame in Cortes de Pallás (Spain) *5th Joint Int. Symp. on Deformation Monitoring (JISDM)* (*Valencia, Spain*, *20–22 June*)
[33] Baselga S, Garcia-Asenjo L, Garrigues P and Lujan R 2022 Dataset for the article GBDM+: an improved methodology for a GNSS-Based Distance Meter *Zenodo* (https://doi.org/10.5281/zenodo.6566948)